Monomer–Dimer Divergent Behavior toward DNA in a Half-Sandwich Ruthenium(II) Aqua Complex. Antiproliferative Biphasic Activity

ARTICLE *in* ORGANOMETALLICS · DECEMBER 2014

Impact Factor: 4.13 · DOI: 10.1021/om5011275

ORGANOMETALLICS

Article

pubs.acs.org/Organometallics

Monomer–Dimer Divergent Behavior toward DNA in a Half-Sandwich Ruthenium(II) Aqua Complex. Antiproliferative Biphasic Activity

Natalia Busto,[†] Marta Martínez-Alonso,[†] José M. Leal,[†] Ana M. Rodríguez,[‡] Fernando Domínguez,[§] M[a] Isabel Acuña,[§] Gustavo Espino,*[,†] and Begoña García*[,†]

[†]Departamento de Química, Facultad de Ciencias, Universidad de Burgos, Plaza Misael Bañuelos s/n, 09001, Burgos, Spain

[‡]Departamento de Química Inorgánica, Orgánica y Bioquímica, Facultad de Químicas, Universidad de Castilla-La Mancha, Avenida Camilo J. Cela 10, 13071, Ciudad Real, Spain

[§]CIMUS, Universidad de Santiago de Compostela, Avenida Barcelona s/n, 15782, Santiago de Compostela, Spain

Supporting Information

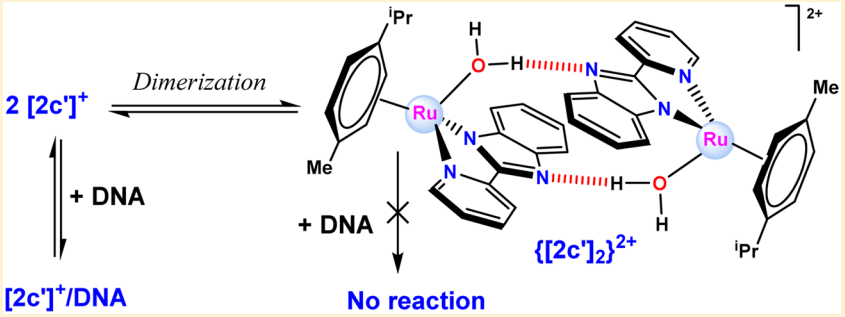

ABSTRACT: The complex $[(\eta^6\text{-}p\text{-cymene})Ru(OH_2)(\kappa^2\text{-}N,N\text{-}HL^1)](OTf)_2$ (HL^1 = 2-pyridin-2-yl-1*H*-benzimidazole), **[2c]-(OTf)$_2$**, undergoes easy deprotonation of the N–H group at physiological pH, producing $[(\eta^6\text{-}p\text{-cymene})Ru(OH_2)(\kappa^2\text{-}N,N\text{-}L^1)]^+$, **[2c′]$^+$**, prone to dimerization both in solution and in the solid state. X-ray measurements on **[2c′]BF$_4$** have shown that dimer units are formed in the solid state by a combination of π–π stacking contacts between the aromatic rings of $[L^1]^-$ and hydrogen bonding involving the water molecules coordinated to the metal center and the deprotonated imidazolyl N atom. The T-jump kinetic curves of the 2D ↔ D_2 equilibrium recorded in the microsecond time scale have allowed us to determine the parameters of the dimerization process. The dimer content diminishes as the ionic strength drops. The different kinetic and thermodynamic techniques have all shown that the monomer reacts with DNA, producing the bifunctional intercalated (through the benzimidazole ligand)-covalent (Ru/N7G) $[(\eta^6\text{-}p\text{-cymene})Ru(\kappa^2\text{-}N,N\text{-}L^1)]$/DNA complex. The cytotoxic activity of **[2c′]$^+$** was evaluated against human lung carcinoma cells (A549) by the MTT cell viability assay. Interestingly, the percentage of surviving cells as a function of the **[2c′]$^+$** content displayed biphasic behavior, interpreted as a result of the rise in the dimer content of **[2c′]$^+$**. As only the monomer can react with DNA, a reasonable correlation between cytotoxic activity and formation of the $[(\eta^6\text{-}p\text{-cymene})Ru(\kappa^2\text{-}N,N\text{-}L^1)]$/DNA complex is established.

INTRODUCTION

Half-sandwich ruthenium(II) arene compounds have been identified recently as an alternative class of potential anticancer drugs that could complement the medicines currently in clinical use, such as cisplatin and its congeners. In particular, several compounds of general formulas $[(\eta^6\text{-arene})RuX(\kappa^2\text{-}N,N\text{-}L)]Y$ have displayed promising anticancer activity.[1] We have assessed recently the cytotoxic activity of ruthenium(II) arene chlorido complexes with 2-aryldiazole ligands,[2] establishing structure–activity relationships, and reported on the synthesis and anticancer properties of other families of bifunctional Ru(II) arene complexes with 2,4-diamino-6-(2-pyridyl)-1,3,5-triazine (2-pydaT) and phenanthroline ligands, verifying that the formation of bifunctional complexes strongly relies on the structure of both the complex and the aromatic ancillary ligand, whereas intercalation of the arene group (*p*-cymene or benzene) was not observed.[3]

None of the complexes investigated so far have shown deviation from the Lambert law that could suggest aggregation in aqueous solution. Aggregation in nonaqueous solution has been reported for amino-acidate half-sandwich ruthenium(II) complexes[4] and cationic half-sandwich Ru(II) complexes bearing neutral N,O-ligands.[5] While self-association of Ru(II) polypyridyl complexes in water has been observed for high Ru(II) complex concentration,[6] aggregation still remains unspecified. Flat aromatic molecules aggregate by stacking caused by a variety of interactions, including hydrophobic

Received: November 10, 2014
Published: December 29, 2014

DOI: 10.1021/om5011275
Organometallics 2015, 34, 319–327

Scheme 1. Synthesis of the Aqua Complexes $[2c](OTf)_2$ or $[2c](BF_4)_2$

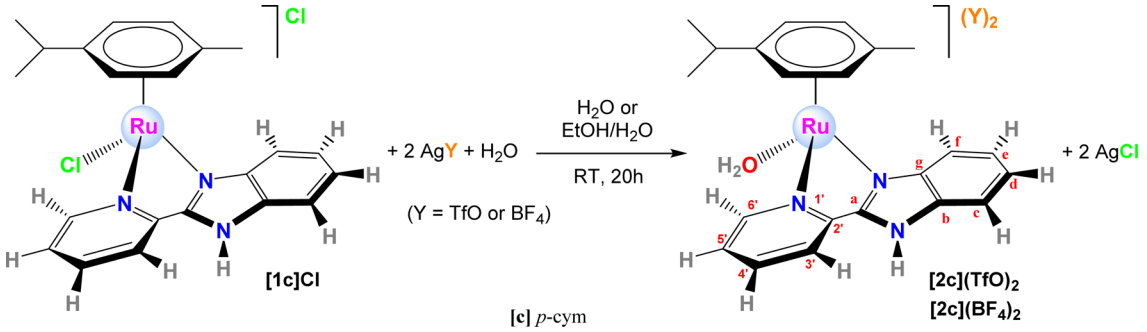

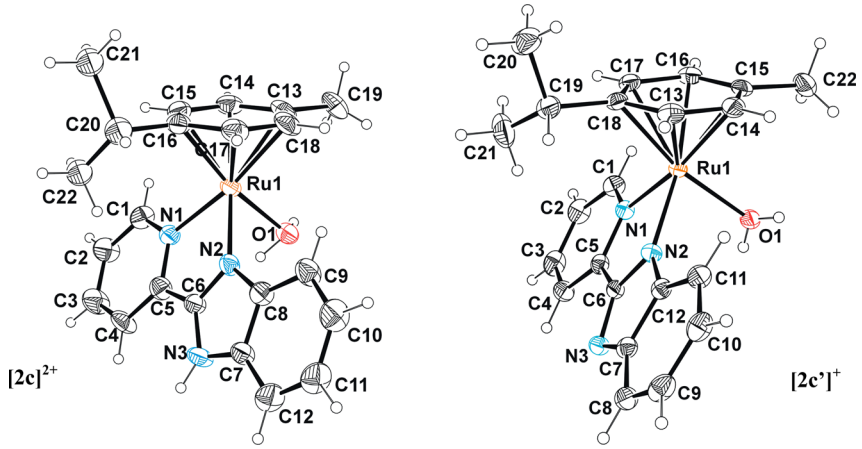

Figure 1. ORTEP diagrams for compounds $[2c](OTf)_2 \cdot H_2O$ and $[2c'](BF_4)$. Counterions and water molecules have been omitted due to space reasons. Thermal ellipsoids are shown at 30% probability.

interactions, dipole−dipole interactions, $\pi-\pi$ interactions, and dispersion forces.

In this work, the dimerization of $[2c']^+$ has been studied in aqueous solution by the kinetic relaxation T-jump technique, calculating the corresponding rate and equilibrium constants, and by X-ray diffraction measurements in the solid state. Also, we have studied the interaction of $[2c']^+$ with calf thymus DNA (CT-DNA), demonstrating the formation of a bifunctional covalent-intercalated complex. Compounds with such dual action (intercalation of the arene group into the DNA bases and metal coordination to DNA) induce an unusual distortion of DNA that affects the recognition by reparation enzymes, leading to apoptosis cell death.[7] Ru-arene complexes with this mode of binding are by far more cytotoxic toward cancer cells compared to the respective non-intercalanting compounds. In view that self-aggregation may affect the physicochemical and biological features of the aqua Ru(II) complex, in the framework of our investigation of dye−nucleic acid interactions we found it interesting to look into the dimerization process prior to studying the DNA interaction as a function of ionic strength. T-jump measurements have shown that only monomer species can interact with DNA, this finding explains the observed biphasic behavior of $[2c](OTf)_2$ cytotoxicity toward lung tumor cells.

RESULTS AND DISCUSSION

Synthesis and Structural Characterization. The monocationic chlorido complexes $[(\eta^6\text{-arene})RuCl(\kappa^2\text{-}N,N\text{-}HL^1)]Cl$, **[1a-c]Cl** (arene = 1-phenoxyethanol, benzene, and *p*-cymene; HL^1 = 2-pyridin-2-yl-1*H*-benzimidazole) convert into the dicationic aqua derivatives $[(\eta^6\text{-arene})Ru(OH_2)(\kappa^2\text{-}N,N\text{-}HL^1)](Y)_2$, $[2a-c](OTf)_2$ or $[2a-c](BF_4)_2$ (Y = OTf^- or BF_4^-), after addition of AgOTf or $AgBF_4$ (molar ratio 1:2) in distilled water or an ethanol/water mixture according to described procedures (see Scheme 1).[2]

X-ray Diffraction. The crystal structures of the dicationic complex $[(\eta^6\text{-}p\text{-cymene})Ru(OH_2)(\kappa^2\text{-}N,N\text{-}HL^1)](OTf)_2$, $[2c](OTf)_2 \cdot H_2O$, and the monocationic derivative $[(\eta^6\text{-}p\text{-cymene})Ru(OH_2)(\kappa^2\text{-}N,N\text{-}L^1)](BF_4)$, $[2c'](BF_4)$, have been elucidated for the first time by X-ray diffraction. A single crystal of $[2c](OTf)_2 \cdot H_2O$ was grown from an aqueous solution by slow evaporation. Single crystals of $[2c'](BF_4)$ suitable for X-ray diffraction were obtained also by slow evaporation from an aqueous solution of its conjugated acid $[(\eta^6\text{-}p\text{-cymene})Ru(OH_2)(\kappa^2\text{-}N,N\text{-}HL^1)](BF_4)_2$, $[2c](BF_4)_2$. We assumed that the two cationic species $[2c]^{2+}$ and $[2c']^+$ are in equilibrium in aqueous media, and thus crystallization of the monocationic specimen most likely occurs due to its lower polarity compared to the dication precursor. The ORTEP diagrams for the two structures are shown in Figure 1, and selected bond lengths and angles with estimated standard deviations are listed in Table 1. For comparison, the corresponding bonding parameters for $[(\eta^6\text{-benzene})Ru(OH_2)(\kappa^2\text{-}N,N\text{-}HL^1)](BF_4)(SiF_6)_{0.5}\}\cdot(H_2O)_2$, $\{[2b](BF_4)(SiF_6)_{0.5}\}\cdot(H_2O)_2$, reported previously,[2] are also listed in Table 1. Relevant crystallographic parameters are given in the Supporting Information (Table S1). The asymmetric units of $\{[2b](BF_4)(SiF_6)_{0.5}\}\cdot(H_2O)_2$, $[2c](OTf)_2 \cdot H_2O$, and $[2c'](BF_4)$ contain just one cation complex. The respective cell units show one or two pairs of the enantiomers R_{Ru} and S_{Ru} resulting from the chiral metal nature of these derivatives. All

DOI: 10.1021/om5011275
Organometallics 2015, 34, 319−327

Table 1. Selected Bond Lengths (Å) and Angles (deg) for Compounds $\{[2b](BF_4)(SiF_6)_{0.5}\}\cdot(H_2O)_2$,[2] $[2c](OTf)_2\cdot H_2O$, and $[2c'](BF_4)$

distance/angle	$\{[2b](BF_4)(SiF_6)_{0.5}\}\cdot 2(H_2O)$	$[2c](OTf)_2\cdot H_2O$	$[2c'](BF_4)$
Ru(1)−O(1)	2.124(3)	2.134(5)	2.122(3)
Ru(1)−N(1)(py)	2.132(4)	2.123(6)	2.114(3)
Ru(1)−N(2)(Im)	2.070(4)	2.082(6)	2.066(3)
N(2)−C(6)	1.333(6)	1.319(8)	1.351(4)
N(3)−C(6)	1.336(6)	1.351(9)	1.333(4)
N(2)−Ru(1)−N(1)	76.79(16)	76.8(2)	76.73(10)
N(1)−Ru(1)−O(1)	82.14(16)	83.9(2)	84.72(12)
N(2)−Ru(1)−O(1)	82.61(15)	81.4(2)	85.55(11)

these cation complexes adopt the classical pseudo-octahedral three-legged piano-stool arrangement, and hence the arene rings display the common π-bonded η^6-coordination mode, whereas the arylbenzimidazole-type ligands assume a bidentate-chelate coordination mode (κ^2-*N,N*). The last place in the coordination sphere is occupied by a water molecule. The Ru−centroid distance for the three complexes is 1.67 Å (Table S1). The Ru−N distance for the benzimidazole heterocycle is shorter than for the pyridyl moiety in all of the cases. Some other geometry parameters are listed in Table S1.

Dimer Entities in the Crystal Structure of Complex $[2c'](BF_4)$. One of the most relevant motifs in the 3D crystal architecture of $[2c'](BF_4)$ is the pairing of enantiomeric isomers through both double $\pi-\pi$ contacts between the aromatic rings of $[L^1]^-$ (py-im/im-py)[8] and the reciprocal strong hydrogen bonds between the coordinated water molecule of each enantiomer as the donor and the deprotonated N atom of $[L^1]^-$ corresponding to the other complex as the acceptor (O1H1A---N3) (see Figure 2 and

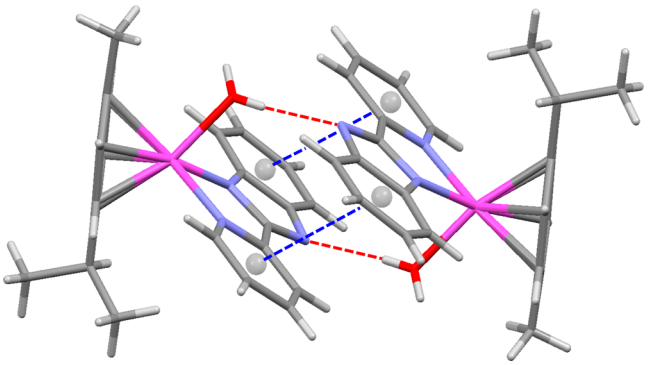

Figure 2. Representation of complex pairing in the $[2c'](BF_4)$ crystal structure. Both $\pi-\pi$ contacts (blue) and hydrogen bonding interactions (red) are involved in the association (Mercury 3.0). The gray spheres represent the centroids of the aromatic rings.

Table S2). Moreover, these dimer entities are connected to each other through linking BF_4^- counterions by means of double hydrogen-bonding interactions, which gives rise to chains along the crystallographic *a* axis.

Determination of the pK_a Values of $[2c](OTf)_2$. The evolution of the absorbance spectra of $[2c](OTf)_2$ as a function of pH reveals a complex behavior (Figure 3A); the isosbestic points recorded unveil different species in equilibrium. The absorbance at λ = 330 nm versus pH plot (Figure 3B), showing two pH values with the same absorbance, indicates that $[2c](OTf)_2$ undergoes two ionization equilibria, thus enabling application of Ang's method[9] to determine the two pK_{ai} values, 5.75 ± 0.04 and 9.15 ± 0.03 (equation and fitting procedure as Supporting Information, Figure S1).

Two different equilibria involving three species can be determined for $[2c](OTf)_2$ (Scheme 2): the $[2c]^{2+}$ dicationic aqua species (prevailing at pH < 5.75), the monocationic conjugate base $[2c']^+$ resulting from N−H deprotonation (prevailing in the 5.75 ≤ pH ≤ 9.15 range), and presumably the neutral hydroxide species $[2c'']$ (pH > 9.15).

We deterined the effect brought about by the coordination of the metallic fragment $[(\eta^6\text{-}p\text{-cymene})Ru(OH_2)]^{2+}$ to the HL^1 ligand on the acidity of the N−H group. According to previous results,[2] two ionization equilibria involving three different species can be established for HL^1, a monocationic species ($[H_2L^1]^+$) in which the pyridyl N is protonated (prevailing at pH < 4.0), a neutral species (HL^1) predominant from pH ≥ 4.06 to pH ≤ 12.50, and an anionic species ($[L^1]^-$) due to deprotonation at the benzimidazole N site (prevailing at pH > 12.50). Therefore, the pK_a value for the deprotonation of the N−H group in HL^1 dramatically dropped from 12.50 to 5.75 as a result of coordination. Summing up, at pH 7.0, in which the DNA binding has been studied, the ligand is present as the (HL^1) neutral form, whereas the prevailing Ru(II) species is the monocationic form, $[2c']^+$ (see Scheme 2). Therefore, the $[2c]^{2+}$ and $[2c']^+$ species set a pH-dependent equilibrium system in aqueous media, in which $[2c']^+$ is the dominant partner at pH = 7.0; hence, from now on we refer to $[2c']^+$ even when using salts of $[2c]^{2+}$ as the starting material for the different experiments.

Dimeric Entities in the Aqueous Solution of Complex $[2c']^+$. To our knowledge, dimers of arylbenzimidazole Ru(II) complexes in aqueous solution have not been reported hitherto. Formation of aggregates can be observed from the variation of the absorbance as a function of the $[2c']^+$ content. Figure 4 plots such variation at I = 0.1 M; the inset shows an increasing $Abs_{242\ nm}/Abs_{210\ nm}$ ratio from $C_D = 2.3 \times 10^{-5}$ M, denoting $[2c']^+$ as D, with the 242 nm band being ascribed to formation of the dimer. For $C_D < 2.3 \times 10^{-5}$, dimers are not observed, and for $C_D > 4.5 \times 10^{-5}$ M precipitation sets in.

Hydrophobic interactions and the presence of salts in solution promote formation of aggregates.[10] Figure 5 shows deviations from Lambert−Beer law at both I = 0.1 M and 2.5 mM ionic strength, indicating that the decrease in the ionic strength drastically lowers the formation of aggregates.

The T-jump kinetic relaxation experiments have also shown the presence of $[2c']^+$ dimers in aqueous solution according to eq 1, where k_f and k_d are the rate constants for dimer formation and dimer dissociation, respectively, with $K_D = k_f/k_d$ being the equilibrium dimerization constant.

$$2D \underset{k_d}{\overset{k_f}{\rightleftharpoons}} D_2 \qquad (1)$$

Proper handling of the T-jump relaxation technique requires the use of high ionic strength (0.1 M); hence, all of the measurements were carried out at pH = 7.0 and I = 0.1 M ($NaClO_4$). The T-jump relaxation technique in the absorbance mode has evinced a fast single-exponential dimerization process of $[2c']^+$ (Figure 6, inset), with $1/\tau_D$ being the kinetic relaxation time.

According to reaction 1, the dependence of the relaxation time on the dye concentration can be expressed in the form

$$1/\tau_D = k_d + 4k_f C_D \qquad (2)$$

DOI: 10.1021/om5011275
Organometallics 2015, 34, 319−327

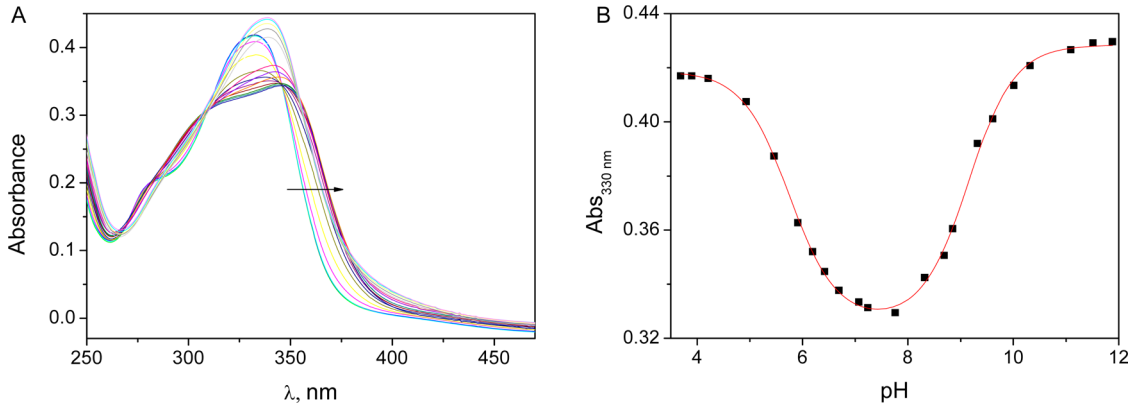

Figure 3. (A) Evolution of the absorbance spectra of $[\mathbf{2c}]^{2+}$ with increasing pH (from 3.5 to 12.0, arrow sense). (B) Absorbance at λ = 330 nm as a function of pH according to eq 6S.

Scheme 2. Dissociation Equilibria for the Aqua Complex $[\mathbf{2c}]^{2+}$

$$[(cym)Ru(OH_2)(HL^1)]^{2+} \;(\mathbf{[2c]^{2+}}) \xrightleftharpoons{pK_{a1} = 5.75} [(cym)Ru(OH_2)(L^1)]^{+} \;(\mathbf{[2c']^{+}}) \xrightleftharpoons{pK_{a2} = 9.15} [(cym)Ru(OH)(L^1)] \;(\mathbf{[2c'']})$$

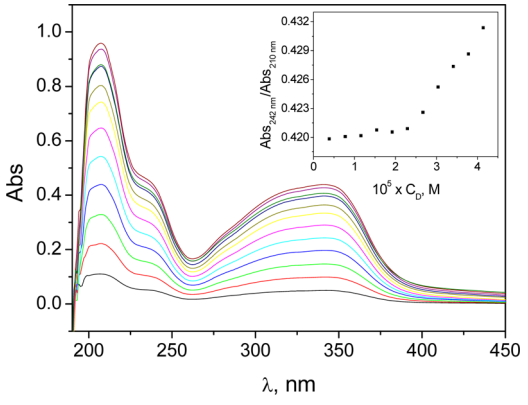

Figure 4. Spectral curves recorded for different $[\mathbf{2c}']^{+}$ concentrations at I = 0.1 M ($NaClO_4$), pH = 7.0 and T = 25 °C. Inset: $Abs_{242\ nm}/Abs_{210\ nm}$ versus $[\mathbf{2c}']^{+}$ concentration plot.

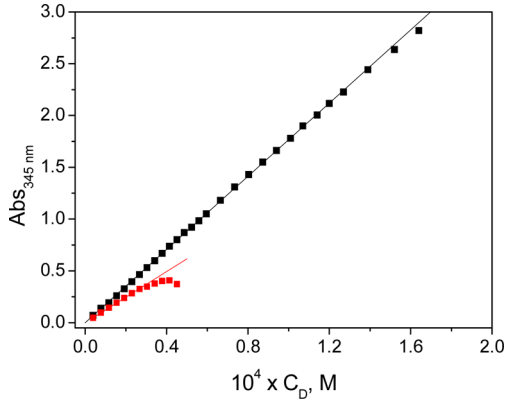

Figure 5. Lambert–Beer law for the $[\mathbf{2c}']^{+}$ complex at (black) I = 2.5 mM and (red) I = 0.1 M ($NaClO_4$). λ = 345 nm, pH = 7.0 and T = 25 °C.

The $1/\tau_D$ versus C_D plot (Figure 6) provides the values k_f = (9.1 ± 1.1) × 10^8 M^{-1} s^{-1}, k_d = (10.2 ± 0.4) × 10^4 s^{-1}, and K_D = (8.9 ± 1.4) × 10^3 M^{-1}. The value obtained for K_D is consistent with the monomer–dimer limits observed spectrophotometrically (Figure 5). Table 2 lists the aggregation parameters compared with those for other antitumor drugs,

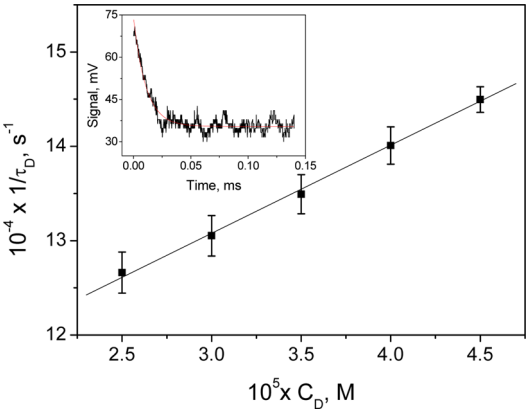

Figure 6. Reciprocal relaxation time for $[\mathbf{2c}']^{+}$ self-aggregation kinetics versus dye concentration; I = 0.1 M ($NaClO_4$), pH = 7.0 and T = 25 °C. The linear trend is based on eq 2, according to the dimerization process. The inset shows a monoexponential relaxation curve C_D = 2.5 × 10^{-5} M and λ = 345 nm.

Table 2. Comparison between Dimerization Reaction Parameters for $[\mathbf{2c}']^{+}$ Self-Aggregation at I = 0.1 M ($NaClO_4$), pH = 7.0 and T = 25 °C

	$10^{-3} \times K_D$, M^{-1}	$10^{-8} \times k_f$, M^{-1} s^{-1}	$10^{-4} \times k_d$, s^{-1}
$[\mathbf{2c}']^{+a}$	8.9 ± 1.4	9.1 ± 1.1	10.2 ± 0.4
TO[b]	31 ± 16	8.0 ± 1.9	2.6 ± 0.7
BO[b]	0.2 ± 0.1		
coralyne[c]	5.2	0.5	1.0
doxorubicin[d]	1.4		

[a]This work. [b]Ref 11. [c]Ref 12. [d]Ref 13

also deduced from T-jump at the same ionic strength. Inspection of Table 2 reveals that K_D has the same order of magnitude as other organic compounds in which π–π stacking interactions prevail, consistent with the dimer entity observed by X-ray diffraction (Figure 2).

DOI: 10.1021/om5011275
Organometallics 2015, 34, 319–327

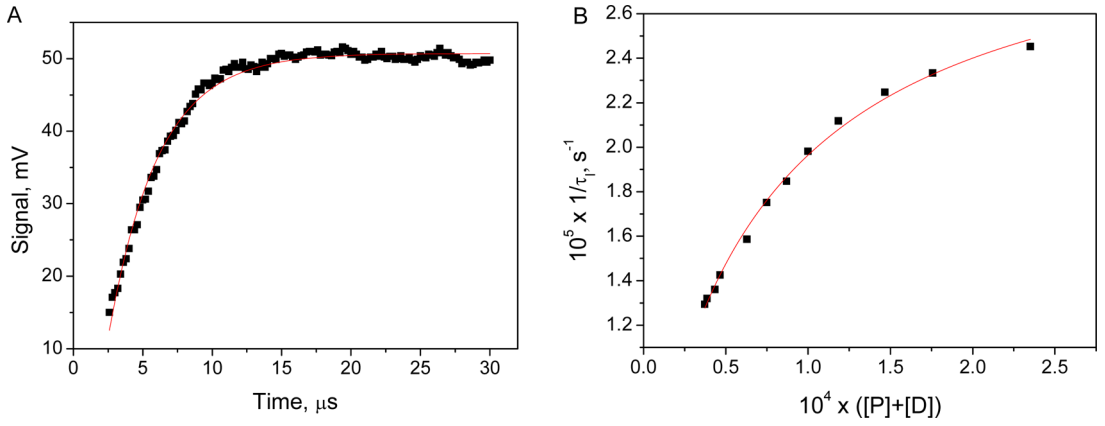

Figure 7. (A) Kinetic curve of $[\mathbf{2c}']^+$/CT-DNA for C_D/C_P= 0.1, λ = 345 nm. (B) Effect of the CT-DNA + $[\mathbf{2c}']^+$ equilibrium concentration on $1/\tau_I$. $C_D = 3.4 \times 10^{-5}$ M, I = 0.1 M ($NaClO_4$), pH = 7.0 and T = 25 °C. Continuous line is the curve fitting.

Table 3. Apparent Binding Constant, K_i, and Formation and Dissociation Kinetic Constants, k_i, Obtained for the $[\mathbf{2c}']^+$/CT-DNA System at pH = 7.0 and T = 25° C

I, M	$10^{-4} \times K_0$, M^{-1}	$10^{-5} \times k_1$, s^{-1}	$10^{-4} \times k_{-1}$, s^{-1}	$K_1 = k_1/k_{-1}$	$10^{-5} \times K$, M^{-1}	$10^3 \times k_2$, s^{-1}
0.1	1.4 ± 0.3	2.9 ± 0.8	2.8 ± 1.4	10.3 ± 1.5	1.6 ± 0.5	
0.0025					22.9 ± 2.0	5.1 ± 0.4

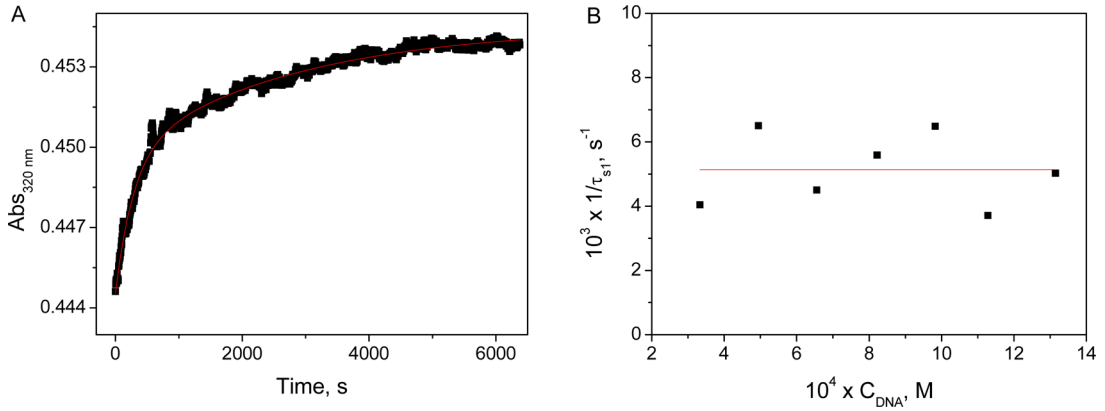

Figure 8. (A) Biexponential kinetic curve recorded at λ = 320 nm, C_D/C_P = 0.1. (B) Effect of the DNA content on the reciprocal relaxation time, $1/\tau s_1$. $C_D = 3.3 \times 10^{-5}$ M, $C_D/C_P \leq 0.1$, I = 2.5 mM, pH = 7.0, and T = 25 °C.

Binding of $[\mathbf{2c}']^+$ and CT-DNA. To elucidate if the biphasic antiproliferative activity (see below) can be related to the DNA binding features, a deeper study on the interaction of $[(\eta^6\text{-}p\text{-cymene})Ru(OH_2)(\kappa^2\text{-}N,N\text{-}HL^1)](OTf)_2$, $[\mathbf{2c}](\mathbf{OTf})_2$, with CT-DNA has been conducted at pH = 7.0 and varying ionic strength (I = 0.1 M and 2.5 mM).

Fast Kinetic Effect: Intercalation. Under excess of DNA (P) (C_D/C_P < 0.1, denoting $[\mathbf{2c}']^+$ as D), the T-jump experiments performed at I = 0.1 M reveal two consecutive relaxation effects with $1/\tau_I$ and $1/\tau_D$ time constants; additionally, in the absence of DNA, the $1/\tau_D$ constant was also observed for the isolated $[\mathbf{2c}']^+$ complex and was related to dimerization (see above). On the basis of the difference between the two time constants, the two kinetic effects were analyzed separately. Regarding the $[\mathbf{2c}']^+$/CT-DNA interaction, Figure 7A displays the relaxation curve recorded at C_D/C_P = 0.1, and Figure 7B the $1/\tau_I$ versus ([P] + [D]) plot, [P] and [D] being the equilibrium concentrations and $1/\tau_I$ the time constant related to intercalation. The observed behavior is consistent with the reaction scheme

$$P + D \overset{K_0}{\rightleftharpoons} PD_0 \underset{k_{-1}}{\overset{k_1}{\rightleftharpoons}} PD_I \quad (3)$$

where the preequilibrium K_0 yields the intermediate PD_0 that evolves to the intercalated PD_I complex, with formation and dissociation rate constants k_1 and k_{-1}, respectively. In line with this finding, the concentration effect on $1/\tau_f$ can be expressed as

$$\frac{1}{\tau_f} = \frac{K_0 k_1([D] + [P])}{1 + K_0([D] + [P])} + k_{-1} \quad (4)$$

K_0, k_1, and k_{-1} are evaluated from fitting of eq 4 to the data pairs (Figure 7B).

From these results, it can be concluded that the overall constant $K = K_0 (1 + K_1)$ is $(1.6 \pm 0.5) \times 10^5$ M^{-1} at 0.1 M and one order higher at 2.5 mM, calculated by the Guggenheim equation[14] (Table 3). The K value lies in the range expected for intercalating ligands.[15]

It should be noticed that, for increasing $[\mathbf{2c}']^+$ content, the amplitude of the T-jump relaxation curves diminished because the dimer species of $[\mathbf{2c}']^+$ are formed at I = 0.1 M and these

DOI: 10.1021/om5011275
Organometallics 2015, 34, 319–327

do not interact with DNA, as shown above. Therefore, the experiments related to the slow interaction with DNA were carried out in the range where the monomer species prevails.

Slow Kinetic Effects: Covalent Binding of [2c′]$^+$ to CT-DNA. Two slow processes were observed from the absorbance spectra recorded over 2 h time for different [**2c**′]$^+$/CT-DNA ratios in at least 10-fold DNA excess. A biexponential model has served to fit the data pairs (Figure 8A), yielding the $1/\tau_{s1}$ and $1/\tau_{s2}$ rate constants. The time constant $1/\tau_{1s} = k_2$ was independent of the DNA content (Figure 8B), evincing that the PD_I intercalated complex (eq 3), observed by T-jump, evolves to the covalently bound PD_{II}; this result, together with the NMR data assembled, in which the Ru(II) site was seen to bind to the N7 of 9-MeG (Figure 9),[2] permits one to assume that PD_{II}

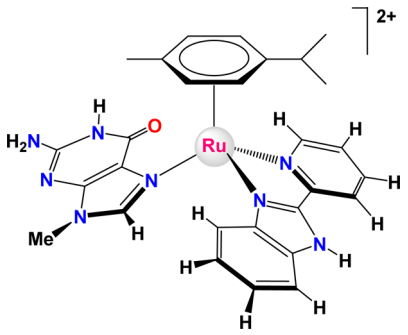

Figure 9. Structure for [(η^6-arene)Ru(9-MeG)(κ^2-*N*,*N*-HL^1)]$^{2+}$.

corresponds to the Ru coordination to the N7 site of the guanine residue. Table 3 collects the formation constant of the coordinated complex, $k_2 = (5.1 \pm 0.4) \times 10^{-3}$ s^{-1}, at $I = 2.5$ mM. PD_{II} will be shown below to bear features of a bifunctional intercalated-covalent complex.

The second relaxation time, $1/\tau_{s2}$, shows a non-well-defined trend (data not shown) with a certain dispersion ascribable to rearrangement of DNA, once the PD_{II} complex is formed. To fully characterize the conformational changes caused by the [**2c**′]$^+$ binding to DNA to produce PD_{II}, viscosity measurements were monitored as a function of time at $C_D/C_P = 0.05$.

The relative viscosity (η/η_0) of the [**2c**′]$^+$/CT-DNA system shows a clear dependence on time, giving rise to single-exponential curves (Figure 10) whose rate constant, $1/\tau = (3.1 \pm 0.2) \times 10^{-3}$ s^{-1}, is close to that obtained by absorbance

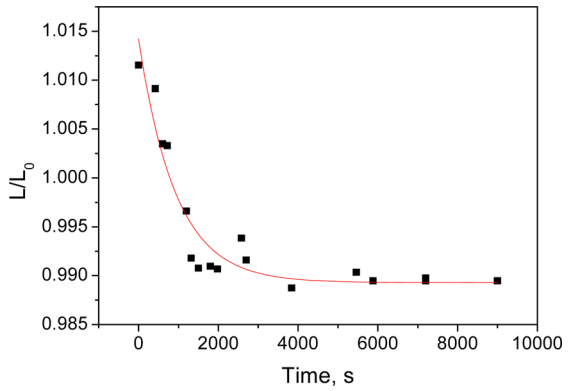

Figure 10. Variation with time of the relative viscosity of a [**2c**′]$^+$/CT-DNA mixture. $C_P = 2.17 \times 10^{-4}$ M, $C_D/C_P = 0.05$, $I = 2.5$ mM, pH = 7.0 and $T = 25$ °C.

measurements. The observed diminution with time of the relative viscosity confirms the covalent binding.[3b]

Thermodynamics: Bifunctional Covalent-Intercalated Complex. The interaction of [**2c**′]$^+$ with CT-DNA has been studied also by a thermodynamic approach. The formation of a bifunctional covalent-intercalated complex (PD_{II}) is confirmed by CD, viscosity, and melting experiments, all of them for different C_D/C_P ratios. Figure 11 shows the CD spectra recorded at different C_D/C_P ratios after a 2 h incubation period, that is, after the Ru(II)−N7G binding was completed.

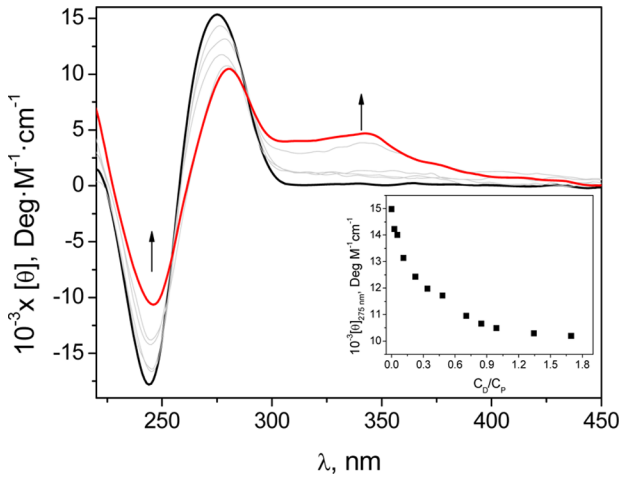

Figure 11. CD spectra of the [**2c**′]$^+$/CT-DNA system recorded after 2 h incubation time at different C_D/C_P ratios. Inset: Molar ellipticity at $\lambda = 275$ nm as a function of C_D/C_P. $C_D/C_P = 0$−1.6, $C_D = 4.13 \times 10^{-5}$ M, $I = 2.5$ mM, pH = 7.0 and $T = 25$ °C.

The intensity of the characteristic negative band of DNA ($\lambda = 245$ nm) decreased as the C_D/C_P ratio was raised, whereas the intensity of the positive band ($\lambda = 275$ nm) not only decreased but also underwent a 5 nm bathochromic shift. This feature is often related to unwinding of the double helix, quite a common effect in intercalation.[16] A new, positive, induced CD band appeared at 345 nm, characteristic of the [**2c**′]$^+$/DNA complex formation, since neither DNA nor [**2c**′]$^+$ displayed any CD signal in that region. The dependence of the molar ellipticity at 275 nm on the C_D/C_P ratio reveals that the binding isotherm bears out the formation of PD_{II}.

Figure 12 shows the change of the contour length of the DNA double helix in the presence of [**2c**′]$^+$. Viscosities were measured for each C_D/C_P ratio: (i) 5 min after the solution was prepared, the least time period needed to complete the viscosity experiment (Figure 12A), and (ii) after 2 h incubation time, to allow formation of PD_{II} (Figure 12B). It should be stressed here that, for a short time period, the viscosity increased up to a maximum for $C_D/C_P \approx 0.2$, reaching $\eta/\eta_0 > 1.0$ up to $C_D/C_P \approx 0.6$. Therefore, the maximum value comes as a result of two opposite effects, namely, increase in viscosity due to intercalation (which prevails for low [**2c**′]$^+$ content) followed by further diminution due to covalent binding. After 2 h incubation (Figure 12B), the covalent binding effect on viscosity prevails and consequently the relative viscosity diminished.

Melting experiments were carried out for different C_D/C_P ratios with fresh solutions (Figure 13). The melting temperature reached a maximum for (roughly) $C_D/C_P \approx 0.2$, close to the maximum observed with viscosity experiments (Figure

DOI: 10.1021/om5011275
Organometallics 2015, 34, 319−327

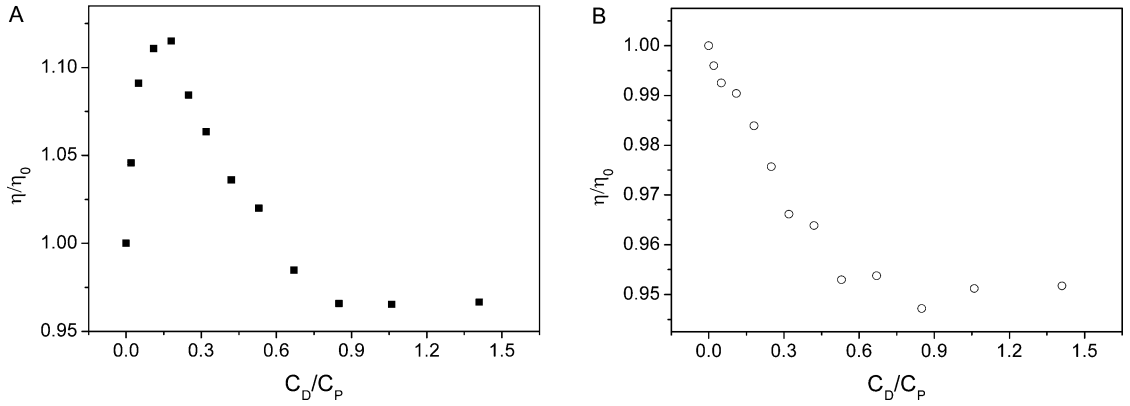

Figure 12. Contour length of the $[\mathbf{2c}']^+$/CT-DNA system as a function of C_D/C_P: (A) fresh solution and (B) after 2 h incubation. $C^0_P = 2.17 \times 10^{-4}$ M, I = 2.5 mM, pH = 7.0 and T = 25 °C.

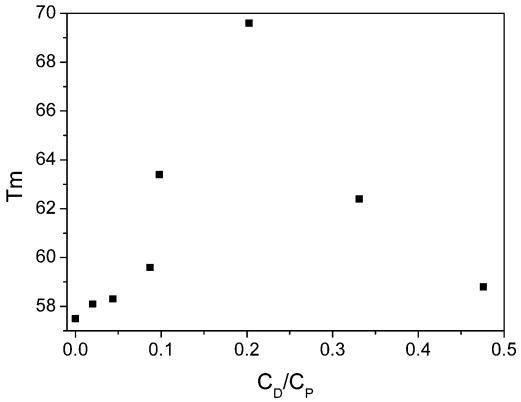

Figure 13. Melting temperature of a $[\mathbf{2c}']^+$/CT-DNA mixture at C_D/C_P = 0–0.47. $C_P = 3.16 \times 10^{-5}$ M, I = 2.5 mM and pH = 7.0.

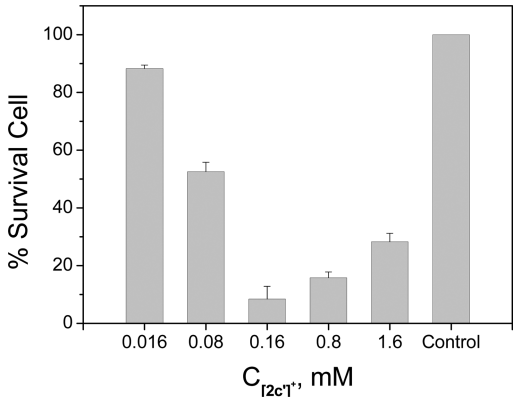

Figure 14. Percentage of surviving cells (A549) as a function of $[\mathbf{2c}']^+$ concentration. The data are an average of five different experiments.

12A). The increase in the melting temperature correlates well with intercalation, showing that for such concentrations intercalation is the prevailing mode of binding.

Lastly, to ensure that covalent binding does not entail deintercalation of the aromatic ligand, new T-jump experiments were conducted at C_D/C_P = 0.1 after 2 h incubation time. Figure S2 demonstrates that intercalation remains upon formation of the Ru(II)/N7G binding and that an equilibrium between the two forms (on-slot and off-slot) of the benzimidazol ligand of $[\mathbf{2c}']^+$ is feasible in the bifunctional covalent-intercalated complex, PD_{II}. Thus, an extended reaction Scheme regarding eq 3 is put forward here (eq 5) involving a new covalent-intercalated complex. The reaction mechanism between $[\mathbf{2c}']^+$ and DNA can then be represented by

$$P + D \overset{K_0}{\rightleftharpoons} PD_0 \underset{k_{-1}}{\overset{k_1}{\rightleftharpoons}} PD_I \rightarrow PD_{II} \quad (5)$$

Cytotoxic Activity. The cytotoxic activity of $[\mathbf{2c}']^+$ was evaluated in the human lung carcinoma cell line A549 by the MTT cell viability assay, using a sample of $[\mathbf{2c}](\mathbf{OTf})_2$ as the prodrug. Interestingly, the percentage of survival cells as a function of the $[\mathbf{2c}']^+$ concentration shows a biphasic behavior (Figure 14). The minimum achieved at 0.16 mM can be explained by the dimerization process described, since at 0.8 mM a noticeable dimer amount is already present in solution at the high ionic strength used in the culture experiments (77% of dimer at I = 0.1 M). Therefore, one can conclude that the dimer is biologically inactive and the monomer is the only cytotoxic agent. Bearing all this in mind, (i) the dimer does not interact with DNA, as evinced from the T-jump kinetic experiments, and (ii) one can conclude that the cytotoxic activity bears relation with the monomer/DNA interaction. This, of course, does not exclude other biological targets. Moreover, the IC_{50} value for $[\mathbf{2c}']^+$ in the A549 cells turned out to be 0.083 mM after an incubation period of 24 h, which compares well with other Ru(II) complexes.[17]

CONCLUSIONS

In conclusion, the biphasic biological activity of $[\mathbf{2c}']^+$ can be related to its interaction with CT-DNA since the dimer species displays no activity either in the MTT assay or in the DNA binding. The study of the binding process between $[\mathbf{2c}']^+$ and DNA by a variety of techniques concludes that $[\mathbf{2c}']^+$ can form dimers in solution, the monomer form giving way to a bifunctional complex at a low drug/DNA ratio with the aromatic ligand intercalated into the DNA of the base pairs and the metal center coordinated to the N7 site of the guanine residues. Such complex formation leads to a thermal stabilization of the DNA double helix.

EXPERIMENTAL SECTION

Materials. The aqueous solutions were prepared with doubly deionized water from a Millipore Q apparatus (APS; Los Angeles, CA, USA). Calf thymus DNA (Sigma-Aldrich) was dissolved in water and sonicated with a MSE-Sonyprep sonicator by applying 20 cycles of 10 s sonication and 20 s pause, at a 98 μm amplitude to suitable DNA samples (10 mL of CT-DNA, 2×10^{-3} M). The sonicator tip was

DOI: 10.1021/om5011275
Organometallics 2015, 34, 319–327

introduced directly into a solution kept in an ice bath to minimize thermal effects. The agarose gel electrophoresis tests performed indicate that the polymer length was reduced to approximately 1000 base-pair fragments. Stock solutions were standardized spectrophotometrically using ε = 13 200 $M^{-1}cm^{-1}$ (expressed in molarity of base pairs) at λ = 260 nm, I = 0.1 M (NaCl), and pH = 7.0 sodium cacodylate. The DNA concentration, expressed in molarity of base pairs, is denoted as C_P. The ionic strength was adjusted using sodium chloride; sodium cacodylate, $(CH_3)_2AsO_2Na$, was used to keep the acidity constant at pH 7.0.

Cell Culture. The human lung carcinoma derived cell line A549 was obtained from Leibniz Institute DSMZ–German Collection of Microorganisms and Cell Cultures. Cells were routinely grown in Dulbecco's modified Eagle's medium (DMEM) (Sigma-Aldrich), supplemented with 10% (v/v) fetal bovine serum (FBS, Gibco-Invitrogen), 1% (v/v) L-glutamine (200 mM, Gibco), and penicillin/streptomycin solution (Gibco).

Methods. *pH Measurement.* The pH values were measured at room temperature using a Metrohm 16 DMS Titrino pH meter fitted with a combined glass electrode and a 3 M KCl solution as a liquid junction, which was calibrated with Radiometer Analytical SAS buffer solutions.

Spectrophotometric Measurements and Thermal Denaturalization Experiments. These were performed on a Hewlett-Packard 8453A spectrophotometer (Agilent Technologies, Palo Alto, CA, USA) fitted out with diode array detection and computer-assisted temperature control systems.

The fast kinetic measurements were performed with a Dialog T-jump instrument built according to the Riegler et al. prototype,[18] in a 1.0 cm path-length cell, working in the absorbance mode. The kinetic curves, collected with an Agilent (Santa Clara, CA, USA) 54622A oscilloscope, were transferred to a PC and evaluated with the Table Curve program of the Jandel Scientific package (AISN software, Richmond, CA, USA). The time constants were averaged from 10-fold repeated kinetic experiments, the observed spread of time constants being 10%.

Viscosity Measurements. These were performed with an Ubbelodhe viscometer (Schott, Mainz, Germany) immersed in a thermostat at 25.0 ± 0.1 °C. The sample viscosity was averaged from triplicate readings of the flow time measured with a digital stopwatch The viscosity data were analyzed using $\eta/\eta_0 = (t - t_0)/(t_{DNA} - t_0)$, where t_0 and t_{DNA} are the solvent and CT-DNA solution flow times, respectively, whereas t is the flow time of the $[\mathbf{2c}']^+$ and DNA mixture. Mean values of replicated measurements were used to evaluate the sample viscosity, η, and that of CT-DNA alone, η_0, the η/η_0 ratio being related to the relative DNA length according to $L/L_0 = (\eta/\eta_0)^{1/3}$.[19]

Circular Dichroism. CD spectra were recorded on a MOS-450 Bio-Logic spectrometer (Claix, France). The measurements were performed at 25 °C in 1.0 cm path-length cells.

MTT Assay and IC_{50} Estimation. A549 cells were plated in a 96-well plate (Iwaki) at 4 × 10^3 cells/well, and 24 h after settlement, the medium was changed for treatment with different amounts of $[\mathbf{2c}']^+$ diluted in culture medium. Thiazolyl Blue tetrazolium bromide, ca. 98% TLC 3-(4,5-dimethyltiazol-2-yl)-2,5-diphenyltetrazolium bromide (MTT) (Sigma), was used to assess cell viability.

X-ray Crystal Structure Determination. Single crystals of $[\mathbf{2c}](\mathbf{OTf})_2\cdot\mathbf{H_2O}$ and $[\mathbf{2c}']\mathbf{BF_4}$ were glued onto the end of a thin glass fiber and transferred to a Bruker SMART APEX CCD-based diffractometer using Mo Kα radiation (λ = 0.710 73 Å). The raw data frames were integrated with the SAINT[20] program and were corrected for Lorentz and polarization effects. An empirical absorption correction based on multiple measurements of equivalent reflections was applied by using the program SADABS.[21] Details of crystal data, data collection, and refinement can be found in Table S2. The structures were solved by a combination of direct methods and difference Fourier synthesis and refined on F^2 by full-matrix least-squares by using the software package SHELXTL version 6.10.[22] Both structures show disorder for the counteranions and were refined over split positions with constrained geometry. The occupancies have been modeled at 50:50. All non-hydrogen atoms were refined with anisotropic displacement coefficients, except those included in the model of disorder for the trifluoromethanesulfonate anions. All hydrogen atoms were added to their geometrically ideal positions except those corresponding to the water molecules and N3 of $[\mathbf{2c}](\mathbf{OTf})_2\cdot\mathbf{H_2O}$, which have been located in the difference map and then fixed. CCDC reference numbers for $[\mathbf{2c}](\mathbf{OTf})_2\cdot\mathbf{H_2O}$ and $[\mathbf{2c}'](\mathbf{BF_4})$ are 1038994–1038995.

■ ASSOCIATED CONTENT

Supporting Information

Additional X-ray tables, Ang's method calculations, and T-jump biexponential curves are available free of charge via the Internet at http://pubs.acs.org.

■ AUTHOR INFORMATION

Author Contributions

The manuscript was written through contributions of all authors. All authors have given approval to the final version of the manuscript.

Notes

The authors declare no competing financial interest.

■ ACKNOWLEDGMENTS

The financial support by Obra Social "la Caixa", project OSLC-2012-007, Junta de Castilla y León (Fondo Social Europeo, project BU-299A12-1), and MICINN projects CTQ2011-24434 and CTQ2009-13051/BQU partially supported by FEDER, Spain, are gratefully acknowledged. We are indebted to J. Delgado, P. Castroviejo, and M. Mansilla, from PCI of the University of Burgos, for technical support.

■ REFERENCES

(1) (a) Süss-Fink, G. *Dalton Trans.* **2010**, *39*, 1673–1688. (b) Bratsos, L.; Jedner, S.; Gianferrara, T.; Alessio, E. *Chimia* **2007**, *61*, 692–697. (c) Sava, G.; Bergamo, A.; Dyson, P. J. *Dalton Trans.* **2011**, *40*, 9069–9075.

(2) Martínez-Alonso, M.; Busto, N.; Jalón, F. A.; Manzano, B. R.; Leal, J. M.; Rodríguez, A. M.; García, B.; Espino, G. *Inorg. Chem.* **2014**, *53* (20), 11274–11288.

(3) (a) Busto, N.; Valladolid, J.; Aliende, C.; Jalón, F. A.; Manzano, B. R.; Rodríguez, A. M.; Gaspar, J. F.; Martins, C.; Biver, T.; Espino, G.; Leal, J. M.; García, B. *Chem.–Asian J.* **2012**, *12*, 788–801. (b) Busto, N.; Valladolid, J.; Martínez-Alonso, M.; Lozano, H. J.; Jalón, F. A.; Manzano, B. R.; Rodríguez, A. M.; Carrión, M. C.; Biver, T.; Leal, J. M.; Espino, G.; García, B. *Inorg. Chem.* **2013**, *52* (17), 9962–9974. (c) Valladolid, J.; Hortigüela, C.; Espino, G.; Busto, N.; Leal, J. M.; Jalón, F. A.; Manzano, B. R.; Rodríguez, A. M.; Carbayo, A.; García, B. *Dalton Trans.* **2014**, *43* (6), 2629–2645.

(4) Ciancaleoni, G.; Di Maio, I.; Zuccaccia, D.; Macchioni, A. *Organometallics* **2007**, *26*, 489–496.

(5) Zuccaccia, D.; Bellachioma, G.; Cardaci, G.; Zuccaccia, C.; Macchioni, A. *Dalton Trans.* **2006**, 1963–1971.

(6) Bhat, S. S.; Kumbhar, A. S.; Lönnecke, P.; Hey-Hawkins, E. *Inorg. Chem.* **2010**, *49*, 4843–4853.

(7) (a) Liu, H.-K.; Sadler, P. J. *Acc. Chem. Res.* **2011**, *44*, 349–359. (b) Bugarcic, T.; Novakova, O.; Halamikova, A.; Zerzankova, L.; Vrana, O.; Kasparkova, J.; Habtemariam, A.; Parsons, S.; Sadler, P. J.; Brabec, V. *J. Med. Chem.* **2008**, *51*, 5310–5319.

(8) Amouri, H.; Caspar, R.; Gruselle, M.; Guyard-Duhayon, C.; Boubekeur, K.; Lev, D. A.; Collins, L. S. B.; Grotjahn, D. B. *Organometallics* **2004**, *23* (19), 4338–4341.

(9) Ang, K.-P. *J. Chem. Phys.* **1958**, *62*, 1109–1112.

(10) (a) Wang, H.; Feng, Q.; Wang, J.; Zhang, H. *J. Phys. Chem. B* **2010**, *114*, 1380. (b) Valdes-Aguilera, O.; Neckers, D. C. *J. Photochem. Photobiol., A* **1989**, *47*, 213. (c) Mooi, S. M.; Heyne, B. *Langmuir* **2012**, *28*, 16524.

DOI: 10.1021/om5011275
Organometallics 2015, 34, 319–327

(11) Biver, T.; Boggioni, A.; Secco, F.; Turriani, E.; Venturini, M.; Yarmoluk, S. *Arch. Biochem. Biophys.* **2007**, *465* (1), 90−100.
(12) Garcia, B.; Ibeas, S.; Ruiz, R.; Leal, J. M.; Biver, T.; Boggioni, A.; Secco, F.; Venturini, M. *J. Phys. Chem. B* **2009**, *113*, 188−196.
(13) Pérez-Arnaiz, C.; Busto, N.; Leal, J. M.; García, B. *J. Phys. Chem. B* **2014**, *118* (5), 1288−1295.
(14) Prue, J. E. *The International Encyclopedia of Physical Chemistry and Chemical Physics*; Pergamon Press, 1966; Topic 15, Vol. *3*, Ionic Equilibria.
(15) Busto, N.; García, B.; Leal, J. M.; Secco, F.; Venturini, M. *Org. Biomol. Chem.* **2012**, *10* (13), 2594−2602.
(16) Busto, N.; García, B.; Leal, J. M.; Gaspar, J. F.; Martins, C.; Boggioni, A.; Secco, F. *Phys. Chem. Chem. Phys.* **2011**, *13*, 19534.
(17) Caruso, F.; Monti, E.; Matthews, J.; Rossi, M.; Gariboldi, M. B.; Pettinari, C.; Pettinari, R.; Marchetti, F. *Inorg. Chem.* **2014**, *53* (7), 3668−3677.
(18) Riegler, R.; Rabl, C. B.; Jovin, T. A. *Rev. Sci. Instrum.* **1974**, *45*, 580−588.
(19) Cohen, G.; Eisenberg, H. *Biopolymers* **1969**, *8*, 45−55.
(20) *SAINT+, Area-Detector Integration Program*, version 7.12a; Bruker AXS Inc.: Madison, WI, 2004.
(21) Sheldrick, G. M. *SADABS, A Program for Empirical Absorption Correction*, version 2004/1; University of Göttingen: Göttingen, Germany, 2004.
(22) *SHELXTL-NT Structure Determination Package*, version 6.12; Bruker AXS Inc.: Madison, WI, 2001.

DOI: 10.1021/om5011275
Organometallics 2015, 34, 319−327